INTERNATIONAL JOURNAL OF AUTOMOTIVE SCIENCE AND TECHNOLOGY

2023, VOL. 7, NO:4, 372-383 www.ijastech.org e-ISSN: 2587-0963

Investigation of Energy Absorbing and Damage Behavior of Gyroid and Diamond Cell Based Lattice Structures Manufactured through Powder Bed Fusion Technology

İsmail Özen[1*] and Mustafa Aslan[2]

0000-0001-9640-7208, 0000-0003-2299-8417

[1] *Department of Mechanical Engineering, Faculty of Engineering, Karadeniz Technical University, Trabzon, 61080, Turkey*
[2]*Metallurgical and Materials Engineering, Faculty of Engineering, Karadeniz Technical University, Trabzon, 61080, Turkey*

Abstract

Cellular porous structures are used as an alternative to blocking structures in industrial fields where multi-functionality and mechanical efficiency are necessary. Many industries, such as automotive, aerospace and defense, utilize the benefits of these structures due to their high specific strength, outstanding noise and vibration damping abilities, thermal shielding, and superior specific energy absorption capacities.

This study aims to reveal energy absorbing behavior and deformation mechanisms under compression load of Gyroid and Diamond cell based triply periodic minimal surface (TPMS) structures manufactured by powder bed fusion (PBF) technology. The TPMS lattice structures fabricated using AlSi10Mg material were designed in different relative densities according to cell wall thickness and cell number. Crushing behaviors of these structures were numerically investigated with a commercial Ls-Dyna finite elements (FE) software. The numerical results were obtained in a good agreement with the experimental data. The FE analysis facilitated understanding of the deformation damage mechanisms and stress distribution on the cell surfaces of the TPMS lattice structures designed with different relative densities. The findings of the study demonstrated that peak stress values computed during crushing of the TPMS lattice structures go up significantly with increasing relative density. Crush force efficiency (CFE) and energy absorption capacity of the TPMS lattice structures remarkably varied depending on deformation damage mechanisms occurred during crushing process. The highest CFE values for the Diamond and Gyroid cell-based lattice structures was obtained as 54% and 51%, respectively. Moreover, it was found that specific energy absorption capacity of the Diamond cell based TPMS lattice structures is 50% more than that of the Gyroid cell based TPMS lattice structures with close relative densities.

Keywords: Specific energy absorption; Finite elements method; Powder bed fusion; Triply periodic minimal surfaces.

Research Article

https://doi.org/10.30939/ijastech..1360762

Received 15.09.2023
Revised 22.11.2023
Accepted 06.12.2023

* Corresponding author
İsmail Özen
ismailozen@ktu.edu.tr
Address: Department of Mechanical Engineering, Faculty of Engineering, Karadeniz Technical University, Trabzon, Turkey
Tel: +904623774513

1. Introduction

Energy absorbing structures are widely used to improve the crashworthiness of vehicles operating in various industrial fields such as automotive, aerospace, and defense. Nowadays, these structures appear as sandwich panels consisting of various types of metallic cellular porous core and surface plates in different engineering applications, thanks to their lightweight and high specific energy absorption capabilities. The sandwich panels can also be preferred due to the ability to provide advantages such as superior energy absorption, outstanding sound, and vibration isolation by using low-density core structures and monolithic surface materials with high bending rigidity [1].

Hybrid sandwich composite panels are employed as a protective shield in armored military vehicles carrying personnel developed by different companies in the defense industry (see Figure 1). These panels are placed on the interior side, ceiling, and floor parts of the vehicle. They behave as secondary energy absorber in front of the main armor to increase the personnel safety against loads

such as crashes or explosions. Vehicle weight, maneuverability, and effective load capacity are important parameters in the design and fabrication of these panels. For this purpose, thanks to light-weight and economical solutions and armor structures that can be easily mounted on the upper, side, and lower floor protections inside the vehicle higher protective levels against threats coming from outside can be achieved than those of STANAG 4569. The possibility of fatal injury is minimized by ballistic helmets and vests containing energy-absorbing materials, as well as using the sandwich panels for the military personnel transported in these vehicles. On the other hand, homogeneous and single-layer ballistic coatings such as armor steel used in armored vehicles carrying military personnel fail to provide sufficient protection in case of any explosion or shock waves. Therefore, this danger can be minimized by using sandwich panels with cellular porous core structures which provide secondary protection against the impact loads in addition to the single-layered armor steel [2].

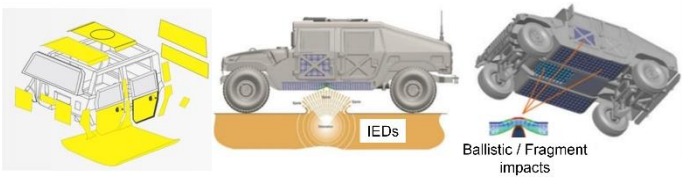

Fig. 1. Application on wheeled armored vehicles of sandwich panels with metal foam and cellular porous core [3].

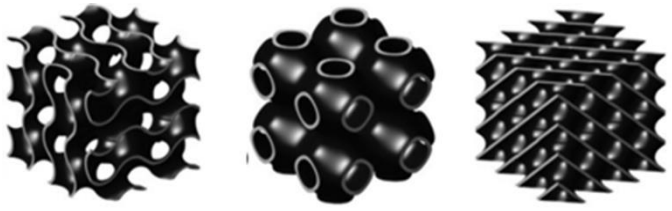

(a) (b) (c)

Fig. 2. Some cell examples of TPMS lattice structures: a) Gyroid, b) Schwarz Primitive, c) Schwarz Diamond cell geometries [6].

Some examples of cellular porous core structures are metallic foams in irregular form and systems that include honeycomb, auxetic, truss and triply periodic minimal surface (TPMS) lattice geometries in regular form. The cell sizes of these structures typically range from 0.1 to 10 mm. The lattice structures with a regular geometry draw attention as being lighter, more rigid, and durable than their foam counterparts. These structures are approximately three times stronger than their foam equivalents. One of the reasons for this difference in strength is that bending is dominant in the foam cell walls, whereas tension and compression are more dominant in the lattice cells. Moreover, it has been reported that the strength of cellular lattice structures under dynamic loading conditions increases due to the microinertia effect [4]. The microinertia effect in TPMS lattice structures is more dominant under dynamic loading conditions, and their strength increases due to the folding damage mechanism occurring during the deformation process [5]. Examples of truss lattice structures include cellular crystallographic (FCC, BCC, FCCZ) and unit cell geometries called tetrahedral beams. Gyroid, Schwarz Primitive, Schwarz and Diamond cell geometries shown in Figure 2 are widely used in TPMS lattice structures.

The TPMS lattice structures consist of closed cells in unlimited connection including minimal surfaces periodically in three directions and have zero average curvatures at each point. Maskery et al. [7] determined that Gyroid celled structures with zero mean curvature surfaces improve energy absorption behavior under compression load. Their results showed that the specific energy absorption capacity of heat-treated double Gyroid (DG) lattice structures up to crushing strain of 50% was approximately three times that of the body centered cubic (BCC) lattice structures examined in a previous study [8]. In another study, the mechanical properties under compressive loading of Gyroid structures manufactured using 3D printer were examined experimentally and numerically. The study's results demonstrated that Gyroid structure has comparable energy absorbing properties to those of Primitive, IWP, and Neovius structures. It was also found that the continuity on the Gyroid cell surfaces doesn't create stress concentrations in the structure [9]. Stiffness and strength properties of the TPMS lattice structures vary depending on relative density, beam or unit cell aspect ratio, unit cell geometry and material properties as well as test loading conditions (static/dynamic) [10]. The TPMS lattice structures show higher specific energy absorption performance compared to metallic foam, auxetic and beam-based cellular truss structures [11–13]. Moreover, the sheet based TPMS structures are superior to solid based TPMS structures in terms of stiffness, strength, and energy absorption properties. Similarly, the energy absorbing capabilities of cellular lattice structures, fabricated using AlSi10Mg powder with an SLM (Selective laser melting) type 3D metal printer were examined in low-velocity (4 m/s) impact conditions. It was concluded that Gyroid cell based TPMS lattice structures show higher penetration depth and energy absorption ability than truss lattice structures (BCC, BCCZ, FBCC, FBCCZ). Furthermore, another advantage of the TPMS based lattice geometries is that they have the same rigidity in all directions [14]. The crushing and crash test studies performed on cellular lattice structures found that the TPMS lattice structures with gradually changing pore ratio absorb higher energy than homogeneous TPMS lattice structures with the same pore ratio.

The TPMS lattice structures can be manufactured using additive manufacturing methods despite their complex geometric designs. For this reason, in recent years, several studies have been carried out on the microstructural properties [15], compressive strength [16] and toughness values [17] of the structures fabricated with 3D metal printers (SLM, SLS, EBM, and DMLS). Many experimental and numerical studies have been carried out on device fabrication parameters, cell patterns of TPMS lattice geometries and relative density (cell wall thickness, cell size and cell direction to volume ratio parameters) regarding samples manufactured by SLM technology using 3D printers [18]. However, especially in the fabrica-

tion of metal structures via this technology, there are some limitations such as high production and device costs, low production velocity, dimensional accuracy, and metallurgical defects [19]. In order to eliminate the defects that arise in the production of cellular lattice structures, there are detailed studies of the effect of processing parameters such as laser speed, laser power, layer thickness, distance between two laser scans in 3D metal printers on the mechanical properties [20]. However, the problems arising during fabrication vary depending on the powder material properties and the applied process parameters. There are limited types of metal powder available for 3D metal printers. Stainless steel (316L) [15], Ti6Al4V [21,22], Inconel 625 [23], AlSi10Mg [24], maraging steel [25] and CP-Ti [26] metal powders are commonly used for the TPMS lattice structure fabrication. Especially in studies done on the fabrication of aluminum alloys through SLM technology, there are some difficulties such as low fluidity [27], high laser reflection, high thermal conductivity [28], and oxidation risk [29].

Determination of the deformation damage mechanisms under static and dynamic loads of the TPMS lattice structures using closed-form analytical equations is limited in terms of engineering applications. It is possible to determine energy absorbing characteristics as well as reveal deformation damage mechanisms in these structures by finite element (FE) analysis. Considering this situation, in this study, firstly, TPMS lattice structures with Gyroid and Diamond cells manufactured by powder bed fusion (PBF) technology using AlSi10Mg alloy material, which is advantageous in terms of lightweight, were tested under compression load. Secondly, commercial Ls-Dyna finite elements software was utilized to reveal energy absorbing characteristics and deformation damage mechanisms throughout the crushing of the TPMS lattice structures designed at different relative densities according to the cell wall number and cell thickness. FE crushing analysis results of the TPMS lattice structures were verified with experimental crash test data. The stress-strain curves, energy absorbing characteristics and deformation damage mechanisms obtained in the result of crushing analyzes were compared with each other.

2. Material and Method

2.1 Design of the TPMS lattice structures

TPMS is a class of mathematically specified surfaces that can be explained by the implicit method. It is also referred level set functions [30]. The functions used to create unit cells of the Gyroid (G) and Diamond (D) cell based TPMS lattice structures are defined as below:

Gyroid cell function:

$$\Phi_G(x,y,z)=\cos(\omega_x * x) * \sin(\omega_y * y) + \cos(\omega_y * y) * \sin(\omega_z * z) + \cos(\omega_z * z) * \sin(\omega_x * x) = 0 \quad (1)$$

Diamond cell function:

$$\Phi_D(x,y,z)= \sin(\omega_x * x) * \sin(\omega_y * y) * \sin(\omega_z * z) + \cos(\omega_x * x) * \sin(\omega_y * y) * \sin(\omega_z * z) + \sin(\omega_x * x) * \cos(\omega_y * y) * \sin(\omega_z * z) + \sin(\omega_x * x) * \sin(\omega_y * y) * \cos(\omega_z * z) = 0 \quad (2)$$

where ω_i is the function period taken account to create the unit cells and calculated as:

$$\omega_i = 2\pi / l_i \quad (3)$$

l_i respectively represents unit cell lengths in x, y, and z directions.

In the present study, Gyroid and Diamond cell based TPMS lattice structures were created in STL (Standard Triangle Language) format by utilizing Mathmod software. The cell geometries of the TPMS lattice structures were created as a surface and exported to in Solidworks CAD program. After these cell geometries were reproduced in the Solidworks CAD program, the TPMS lattice structures designed for this study were drawn as 3D solid model. Then, the TPMS lattice structure designs used in the tests were fabricated by processing in the 3D metal printer. The TPMS lattice structure samples were cut as symmetrical in sizes of 50 mm x 50 mm x 25 mm to reduce the analysis time and fabrication costs. One of the original aspects of this study is to determine the effect on relative density of cell wall thickness and cell number. Therefore, the TPMS lattice structures were designed in three different relative densities using the same cell sizes.

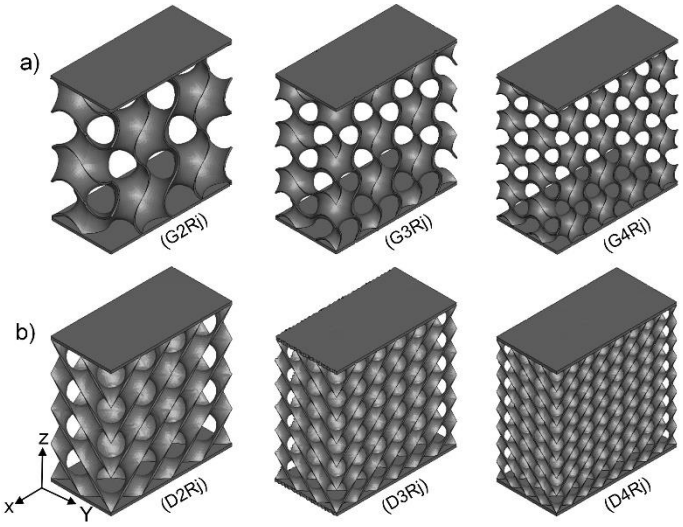

Fig. 3. Designs of Gyroid (a) and Diamond (b) celled TPMS lattice structures (j=1, 2, 3).

The design parameters in terms of relative density of the Gyroid and Diamond cell based TPMS structures are given in Table 1. 3D designs according to cell numbers of these structures are shown in Figure 3. Relative density is a very important design parameter in terms of performance evaluation for TPMS lattice structures [31]. Relative density of a lattice structure is the ratio between its cellular porous volume and cubic bounding box, and it is calculated as

follows:

$$\overline{\rho} = \frac{m_s}{m_b} \quad (4)$$

where m_s is lattice structure mass and m_b is mass of the cubic bounding box.

The relative density values according to unit cell dimensions (wall thickness, width, and height) of the TPMS lattice structures can be obtained from their FE crushing models. As a result, the relative density of the TPMS lattice structures depends on the cell wall thickness, as seen from Table 1. From here, it can be understood that there is a linear relationship between the relative density and cell wall thickness. It is possible to manufacture the TPMS structures designed for this study in practice. For the specific energy absorption value at the desired level, relative density values that vary depending on cell wall thickness and number of cells have been generally preferred in the range from 7% to 30% in the literature studies [21,31,32].

Table 1. Relative densities based on cell design parameters of the TPMS lattice structures.

Cell geometry	Cell numbers	Thickness (mm)	Width (mm)	Height (mm)	Relative density (%)	Cell label
Gyroid	2 x 2 x 1	0.6	25	25	7.4	G2R1
		0.9	25	25	11.2	G2R2
		1.2	25	25	14.8	G2R3
	3 x 3 x 1.5	0.4	16.7	16.7	7.4	G3R1
		0.6	16.7	16.7	11.2	G3R2
		0.8	16.7	16.7	14.8	G3R3
	4 x 4 x 2	0.3	12.5	12.5	7.4	G4R1
		0.45	12.5	12.5	11.2	G4R2
		0.6	12.5	12.5	14.8	G4R3
Diamond	2 x 2 x 1	0.6	25	25	9.2	D2R1
		0.9	25	25	13.8	D2R2
		1.2	25	25	18.4	D2R3
	3 x 3 x 1.5	0.4	16.7	16.7	9.2	D3R1
		0.6	16.7	16.7	13.8	D3R2
		0.8	16.7	16.7	18.4	D3R3
	4 x 4 x 2	0.3	12.5	12.5	9.2	D4R1
		0.45	12.5	12.5	13.8	D4R2
		0.6	12.5	12.5	18.4	D4R3

2.2 Fabrication of the TPMS lattice structures

G2B1 and D2B1 labeled TPMS lattice structures were fabricated using a 3D metal printer (EOS M290). The direct metal laser sintering (DMLS) method, a special additive manufacturing method utilizing powder bed fusion (PBF) technology, were employed in fabrication process. The fabrication process parameters are shown in Table 2. AlSi10Mg powder, which is supplied by EOS Aluminum Company (Germany), with an average diameter of 43 μm, was used for this fabrication process (see Table 3). To improve fabrication quality of the 3D metal printer, the oxygen content was kept below 0.1% and the platform temperature was set to 180°C. The TPMS lattice structure samples were removed from the substrate via the EDM (Electro Discharge Machining) process to obtain a smooth surface quality and decrease the stress concentration effect. Afterwards, the specimens were exposed to a heat treatment process at 500 °C for 4 hours to reduce the effect of residual stresses.

2.3 Material characterization

To obtain the mechanical properties of the AlSi10Mg alloy specimen, tension tests were conducted with an MTS universal testing machine with load measuring capacity of 100 kN. The mechanical properties obtained from the tensile test were used as material properties for the FE crushing model of the TPMS lattice structures. Three tensile specimens were manufactured with the DMLS method under the same conditions according to the ASTM-E8/E8M standard [33]. The effective stress-effective plastic strain curve of the AlSi10Mg alloy material, which was obtained from the tension tests, is depicted in Figure 4. Moreover, the mechanical properties of the AlSi10Mg alloy material are listed in Table 4.

Table 2. Parameters for the PBF fabrication process.

Parameter	Value
Average powder diameter (μm)	43
Laser power (watt)	200
Layer thickness (μm)	25
Hatch distance (μm)	130
Scanning speed (mm/s)	500

Table 3. Chemical contents of the AlSi10Mg powder.

Material	Al	Si	Cu	Mn	Mg	Zn	Fe
AlSi10Mg powder Wt%	Res.	9-11	≤0.05	≤0.45	0.25-0.45	≤0.1	≤0.55

Table 4. Material properties of the AlSi10Mg alloy specimen.

Density (g/cm^3)	Young modulus (GPa)	Poisson's ratio	Yield strength (MPa)
2.65	68.5	0.33	242.71

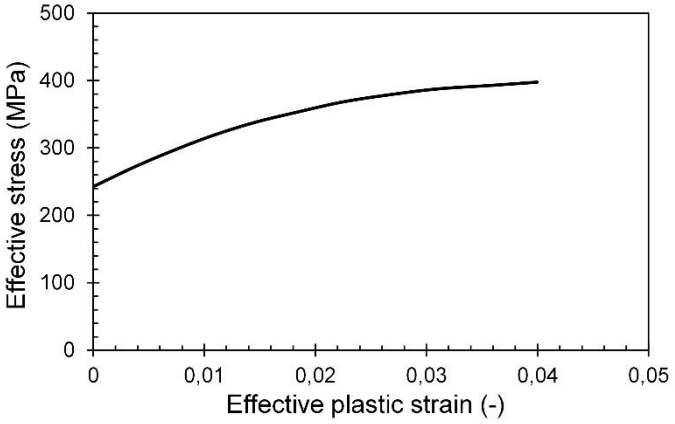

Fig. 4. Effective engineering stress curve versus effective plastic strain of the AlSi10Mg alloy specimen.

2.4 Crushing test

Crushing tests of the TPMS lattice structures under quasi-static compressive loads were carried out using the MTS universal testing machine. The loading plate was set to a constant velocity of 1 mm/min at room temperature (see Figure 5). A camera system was used to take images of the deformations that occurred in the samples throughout the test. The stress (engineering stress, σ) value was calculated by dividing reaction force on the loading plate by the top cross-section area of the TPMS lattice structure samples. The strain (engineering strain, ε) value was obtained by dividing the crushing distance in the loading direction by the initial height (50 mm) excluding the upper and lower surface plates of the TPMS lattice samples [34].

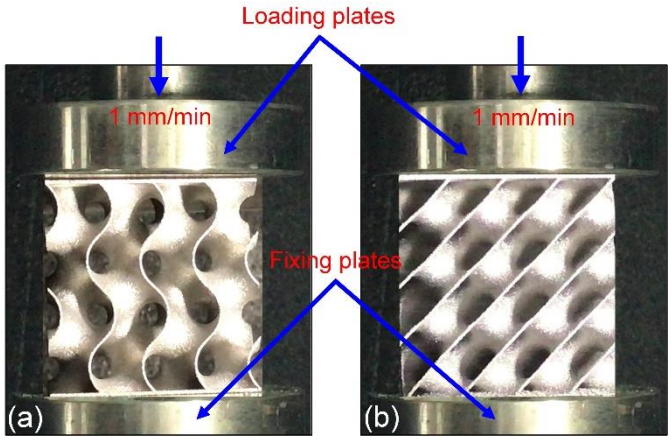

Fig. 5. Crushing test setup of the TPMS lattice structures: a) G2B1 labeled Gyroid and b) D2B1 labeled Diamond samples.

2.5 FE crushing model of the TPMS lattice structures

A commercial Ls-Dyna finite element software was employed to numerically model crushing behavior of the TPMS lattice structures under compression load. Since the Gyroid and Diamond cell based TPMS lattice structures have complex surface geometry, it is very laborious and time-consuming to model as solid of these structures using general CAD programs. Therefore, firstly, the surfaces of these TPMS lattice structures were drawn using Mathmod software [35] and exported to the SolidWorks' CAD program after saving them in STL format. After 3D solid models of these TPMS lattice surfaces were created in the SolidWorks CAD program, these models were imported in the Ls-Dyna program.

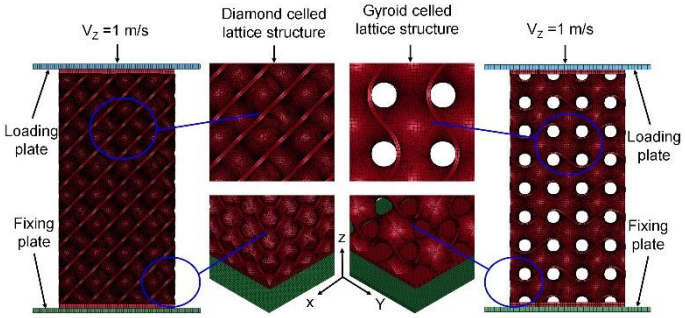

Fig. 6. FE crushing models of the Gyroid and Diamond celled lattice structures.

Figure 6 shows the details with boundary conditions and mesh structure of the FE crushing model created in the Ls-Dyna program. Since the ratio of cell wall thickness to other sizes (cell, width, and height) of the TPMS lattice structures is not small enough (<0.1), solid elements (element formulation = 1) were used in FE crushing models of these structures. Shell elements with 4 nodes (element formulation = 2) were implemented on the loading and fixing plates. Since the TPMS lattice structures have functionally defined curved surfaces, triangular prism elements were used in the finite element model of these structures [36]. To eliminate the effect of the mesh element size on the FE analysis results, FE crushing analyses were carried out with the most appropriate mesh element sizes, confirming the experimental results. Therefore, element sizes in the range of 0.3-0.6 mm for the G2RJ and D2RJ designs, 0.2-0.4 mm for the G3RJ and D3RJ designs, and 0.15-0.3 mm for the G4RJ and D4RJ designs were chosen to ensure converging independently from the mesh. However, smaller element sizes were not preferred as they would increase solution cost of the FE analyses considerably.

To determine the deformation damage mechanisms of the TPMS lattice structures with AlSi10Mg alloy material, the MAT24 (Piecewise Linear Plasticity) material card, which considers elastoplastic damage effects, was employed in the FE model. The MAT24 material card involves one effective failure strain parameter for element damage, and it also takes into account strain rate effects [37]. Since the tests under tensile and compression of specimens fabricated using AlSi10Mg material were performed at

very low loading speeds (1 mm/min), strain rate effects of this material were not considered in the FE crushing analyses. The Poisson's ratio, elasticity modulus, yield strength values given in Table 4 and the effective stress curve versus effective plastic strain shown in Figure 4 were used as input parameters for the MAT24 material card. The effective failure strain parameter for the AlSi10Mg material was taken as 0.12. This parameter was verified by comparing the FE analysis and test results of the TPMS lattice structures under quasi-static compressive load.

Contact algorithms were used to provide interactions with loading/fixing plates of the TPMS lattice structure surfaces involving in the FE model. Therefore, "Automatic Surface to Surface" and "Automatic nodes to Surface" contact algorithms were defined between the loading / fixing plates and the TPMS lattice structures. Additionally, "Eroding Single Surface" contact was applied to the TPMS lattice structures to activate damage occurring in case of self-contact during folding of the cell surfaces. Static friction coefficient for all contact interfaces was assumed 0.3 as reported in the literature [38–40]. As shown in the Figure 7, the experimental and numerical deformation images are compatible with each other. Therefore, it was also accepted as 0.3 in the FE analyses of the other TPMS lattice structures. Since a constant loading velocity of 1 mm/min took too much time for an explicit solution in the FE crushing analysis, a constant velocity of 1 m/s was applied to the loading plate [39]. Moreover, the mass scaling (material density multiplied by 100) approach was applied to the FE crushing models to reduce the solution time [41].

3. Results and Discussion

3.1 Validation of the FE crushing models of the TPMS lattice structures

The stress-strain curves and deformation images determined from the crushing tests of G2B1 and D2B1 labeled TPMS lattice structures were benchmarked to verify the FE crushing analysis results, as shown in Figure 7. One of the possible reasons for the deviations among the numerically and experimentally designated stress-strain curves is that isotropic material properties could not be ensured homogenously at all cells of the TPMS lattice structures during fabrication. In other words, geometric defects such as residual powder particles adhering to the surface, surface roughness, pores, and uneven thickness of layer-based structures can influence the mechanical behavior of the TPMS lattice structures [42]. Furthermore, deviations between the numerically and experimentally detected stress-strain curves were more dominant in the Diamond cell based TPMS lattice structure due to more drooping joints and surfaces among the two-unit cells, which can be referred to a higher possibility of causing stress concentration [43,44]. As seen in the Figures 7, 8, and 10, the maximum stress values were obtained in the regions where stress concentrations occurred during the crushing analysis of the TPMS lattice structures, and these regions are colored in red. Brittle damaged fractures occurred in regions with the stress concentration.

Compared to the numerically and experimentally found stress curves versus strain of the TPMS lattice structures, the FE crushing model has different degrees of susceptibility to the defects of various cell-based lattice structures manufactured by the DMLS method. The stress weakening in the plateau region of both TMPS lattice structures was at different levels. In contrast, the attenuation level obtained from the FE crushing analyses was lower. This situation was ascribed to the presence of different levels of microdefects in the DMLS fabricated TPMS structures. Considered compatibility between the experimental and numerical results, it can be concluded that the FE crushing model adequately predict the energy absorption and damage behavior of the TPMS lattice structures. Therefore, the energy absorbing characteristics and deformation damage mechanisms of the TPMS structures designed with different cell parameters can be revealed and optimized by the FE crushing analyses.

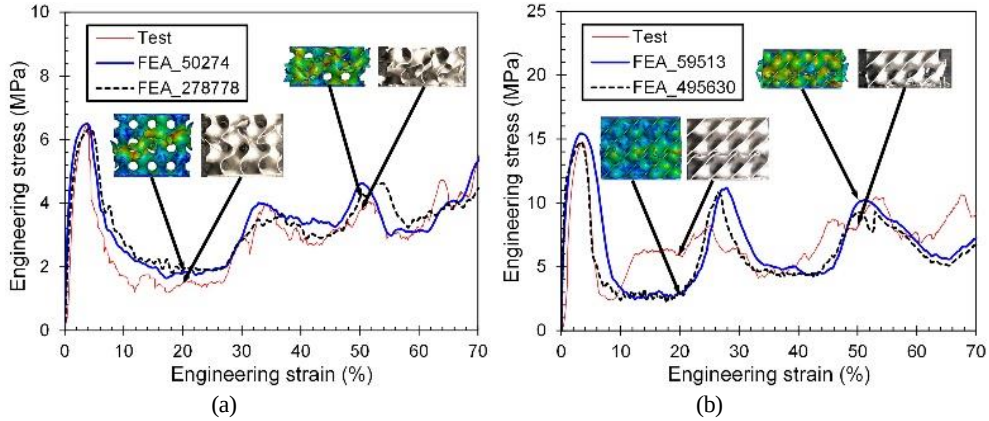

Fig. 7. Benchmark of the experimental and numerical stress-strain curves with the deformation mechanisms of the TPMS lattice structures throughout the crushing process: a) G2B1 labelled Gyroid, and b) D2B1 labelled Diamond samples.

The experimental and numerical stress-strain curves of G2B1 and D2B1 labeled TPMS lattice structures are in a good agreement at elastic and plateau regions. This demonstrates that the experimental results can be verified numerically, and mesh structure used in the FE crushing models is independent of the element size. As seen in the Figure 7, the numerical stress-strain curves of the TPMS lattice structures for two different mesh structures are compatible with each other. After mesh convergence provided for the analyses, the FE crush analyses were continued with the most ideal mesh sizes that we adopted to decrease analysis time. Thus, it is predicted that the FE crushing analysis results of the Gyroid and Diamond cell based TPMS lattice structures, which are designed according to different relative densities, may be compatible with the experimental results. Based on this prediction, the studies were continued with the FE analyses to determine relative density effect of the TPMS lattice structures based on the cell wall thickness and cell size.

As can be seen from Figure 7a, according to numerically and experimentally obtained deformation images taken at 20% and 35% crushing strains of the G2B1 labeled TPMS lattice structure, fractures in the cell folding locations occurred because of brittle material damage behavior. On the other hand, from the experimental and numerical deformation images obtained at 20% and 35% crushing strains of the D2B1 labeled TPMS lattice structure shown in Figure 7b, brittle fractured damage started in its middle cells and continued until damaging adjacent cells. Due to these fractures, fluctuations occurred in the plateau region of the stress-strain curve of the TPMS lattice structures. According to deformation images obtained from the FE crushing analyses, while the von Mises stress values were at maximum levels (red colored regions) on the damaged surfaces, these values were at minimum levels (blue colored regions) on non-damaged surfaces.

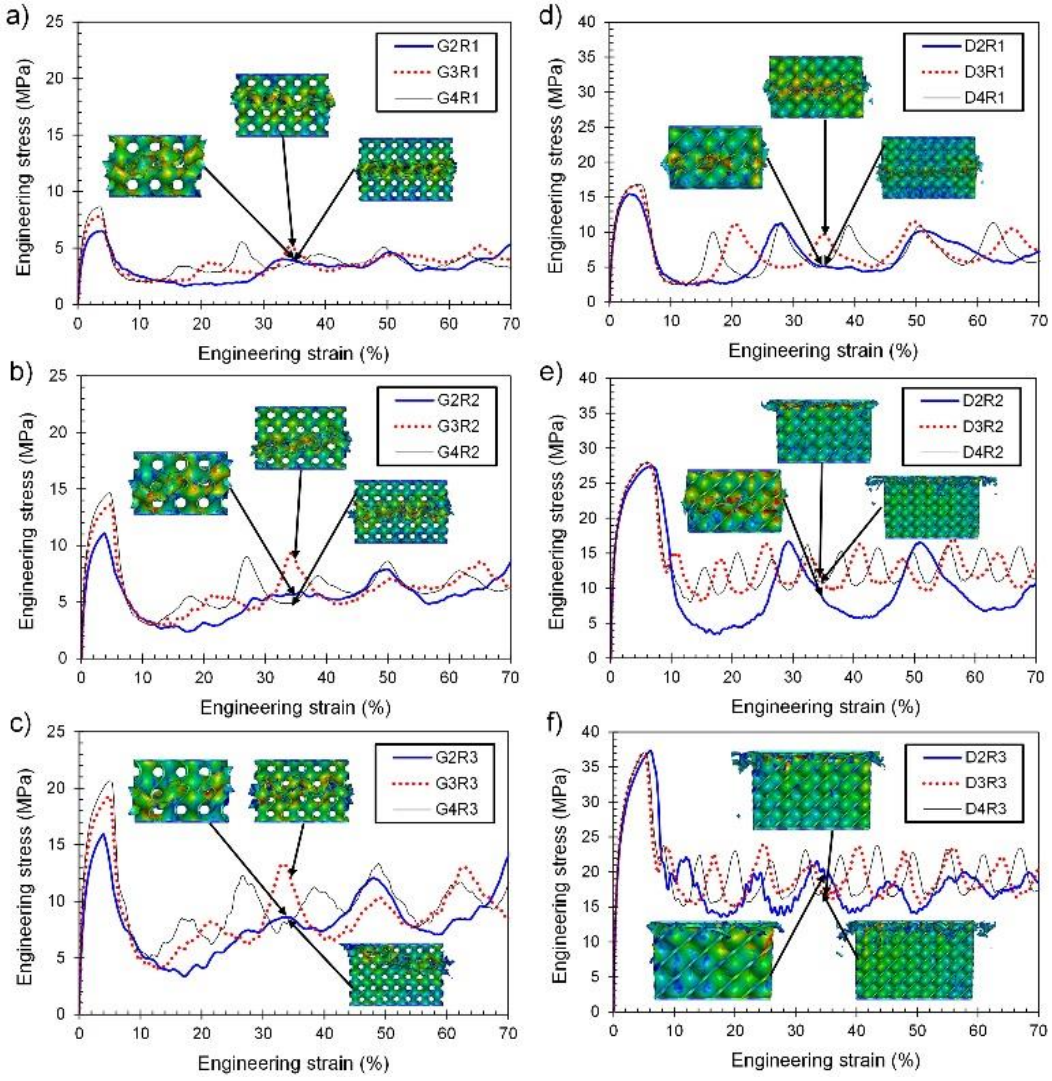

Fig. 8. Comparison of numerically obtained engineering stress-strain curves under compressive load of the TPMS lattice structures designed according to the cell wall thickness and number at different relative densities: a) 7.4% Gyroid, b) 11.2% Gyroid, c) 14. 8% Gyroid, d) 9.2% Diamond, e) 13.8% Diamond, and f) 18.4% Diamond

3.2 Crushing response of the TPMS lattice structures

The crushing response of the TPMS lattice structures designed at various relative densities based on cell number and cell wall thickness has been numerically revealed. The stress-strain curves detected from the FE crushing analyses of the TPMS lattice structures are given comparatively in Figure 8. While peak stress values were obtained at strains varying in range from 4% to 5% in the Gyroid cell based TPMS lattice structures, these values in the Diamond cell based TPMS lattice structures were obtained at strains changing between 5% and 6%. There were sudden decrements in the stress values until the beginning of the plateau zone of the TPMS lattice structures due to the brittle fracture damages on the cell walls. According to the images obtained at the strain instants of 35% shown in Figure 8, the folding damage mechanism in the cells of the TPMS lattice structures led to an increment in the number of fluctuations in the stress-strain curves based on increasing cell number. The peak stress values of the TPMS lattice structures went up significantly with increasing relative density due to an increment in cell wall thickness. In the case of constant relative density, there was a significant increase in the peak stress values due to the increment in the number of cells in the Gyroid cell based TPMS lattice structures, whereas these values changed negligibly in the Diamond cell based TPMS lattice structures.

3.3 Energy absorbing characteristics of the TPMS lattice structures

Specific energy absorption (SEA) capability gives important ideas to benchmark crashworthiness performance of energy absorbing structures [38]. The SEA is the energy capacity absorbed per unit mass (m) of energy absorbing structures and is defined as

$$SEA = \frac{EA}{m} \tag{5}$$

Energy absorption (EA) is the region under the force-displacement curve up to the densification region during crushing and it is calculated by integrating the load corresponding to the crushing distance (δ) up to the total crushing distance (δ_T) as below:

$$EA = \int_0^{\delta_T} F(\delta) d\delta \tag{6}$$

The mean crush force (MCF) is an important design parameter used to reveal the energy absorbing ability of a structure. If the MCF value of the structure goes up, its energy absorption capacity boosts at the same ratio. The MCF is the ratio of energy absorption capacity of the structure to its total crushing distance and calculated as:

$$MCF = \frac{EA}{\delta_T} \tag{7}$$

Crushing force efficiency (CFE) is a critical design parameter regarding the effectiveness of the peak crush force (PCF) in the plateau region of the crushing stress-strain curve. The CFE gives important ideas related to the energy absorption performance of the structures. It is the ratio of the mean crush force to the peak crush force and is defined as

$$CFE = \frac{MCF}{PCF} \tag{8}$$

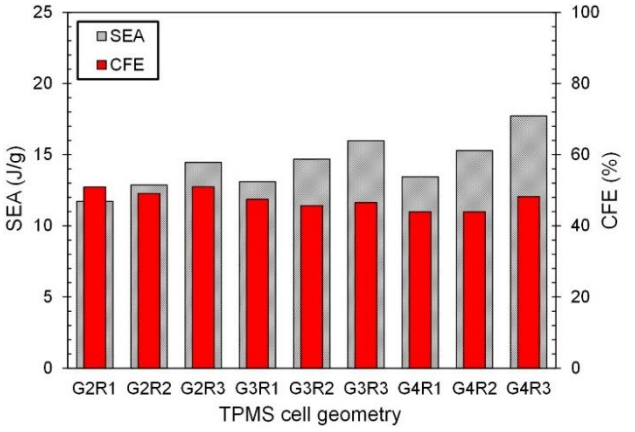

(a)

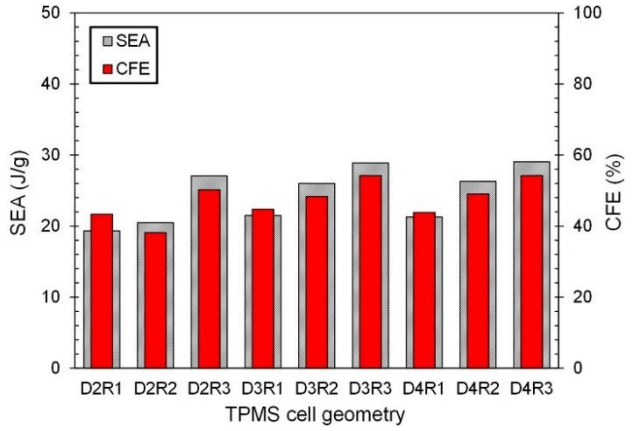

(b)

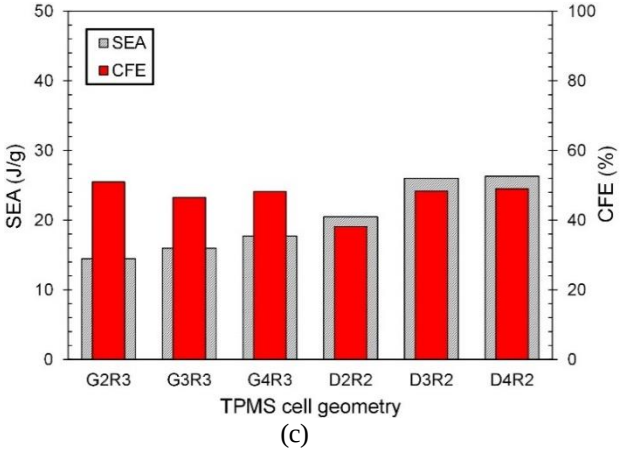

(c)

Fig. 9. Benchmark of SEA and CFE characteristics based on relative density of the TPMS lattice structures: a) Gyroid cells, b) Diamond cells designed at different relative densities, and c) Gyroid and Diamond cells designed at close relative densities.

In the present study, the CFE and SEA characteristics were used as criteria to compare the crashworthiness performance of the TPMS lattice structures. These characteristics were calculated for the region up to 70% strain, where the densification zone of the stress-strain curve starts.

Comparisons of the specific energy absorption (SEA) and crush force efficiency (CFE) characteristics of the TPMS lattice structures are given in Figure 9. Crush force efficiency (CFE) of the TPMS lattice structures remarkably varied depending on deformation damage mechanisms occurred during crushing process. As seen in Figure 8(b, c), there were increases in CFE values due to the progressive deformation damage mechanism occurred in Diamond cell lattice structures due to the increase in relative density. On the other hand, in the designs with low relative density (see Figure 8a), CFE values of the Diamond cell based lattice structures were obtained lower than those of Gyroid cell based lattice structures as catastrophic damage initially occurred in the middle cells. The highest CFE values were obtained as 51% in the G2R1 labeled structure, whereas the lowest CFE value was calculated as 44% in the G4R1 and G4R2 labeled structures (see Figure 9a). While the highest CFE value were 54% in the D3R3 and D4R3 labeled structures, the D2R2 labeled structure had the lowest CFE value as 38%, as seen in Figure 9b. However, the SEA values of the TPMS lattice structures went up with boosting relative density based on cell wall thickness. Moreover, the SEA values of the TPMS lattice structures increased with increasing cell number under constant relative density (see Figure 9c). The highest SEA values in the Gyroid cell based TPMS lattice structures were obtained in GiR3 (i=2, 3 and 4) labeled structures with 14.8% relative density. The SEA values for the G4R3, G3R3 and G2R3 labeled structures were calculated as 17.7 J/g, 16.0 J/g and 14.5 J/g, respectively. For the Diamond cell based TPMS lattice structures with D4R2, D3R2 and D2R2 label with 13.8% relative density, these values were obtained as 26.3 J/g, 26 J/g and 20.5 J/g, respectively. As can be understood from these results, the Diamond cell based TPMS lattice structures showed 50% more specific energy absorption performance than the Gyroid cell based TPMS lattice structures with close relative density.

3.4 Damage behaviors of the TPMS lattice structures

Figure 10 depicts the damage mechanisms and stress distributions obtained on the cell surfaces at different crushing strains (5%, 20%, 35%, and 50%) in the result of the FE crushing analysis of the Gyroid and Diamond cell based TPMS lattice structures designed with relative densities of 14.8% and 13.8%, respectively. It can be seen from Figures 8(c, e) that deformation damage mechanisms changed with an increment at relative density based on the cell wall thick-ness for the same cell geometry. As a result, these deformation damage mechanisms are highly dependent on both the cell wall thickness and cell geometry. The Gyroid cell based TPMS lattice structure with lower cell numbers (G2R3) exhibited a damage mechanism in the form of shear to the left due to the brittle fractured damage behavior after 20% deformation strain (see Figure 10a). However, after the peak stress in the G3R3 labeled TPMS lattice structure, a folding damage mechanism appeared in the middle cells (see Figure 10b). During the crushing strain of 5%, the damaged Gyroid cell surfaces had maximum stress levels. However, as the crushing strain increased, the Gyroid cell based TPMS lattice structures entered the yield zone and the stress levels decreased. After the shear and folding damage mechanisms occurred, the cells fractured diagonally. Meanwhile, cracks developed and progressed towards to nondamaged cells due to the fractures occurred in the Gyroid cells. When the crushing strain reaches up to 20%, the folding damage mechanisms formed in the twist places of the Gyroid cells. In the case of 35% crushing strain, half of the Gyroid cells damaged and folded over each other. On the other hand, during the crushing of the Gyroid cell based TPMS lattice structures, the cell walls had brittle fractured damage mechanisms. In the G4B3 labeled TPMS lattice structure, a progressive damage mechanism appeared starting from the upper left edge and continuing as a shift to the right at the crushing strains in the range from 20% to 35% (see Figure 10c). Moreover, a horizontal layer fracture occurred in some cells due to an increment in the cell number. As a result, the progressive damage mechanism led to increase the specific energy absorption capacity in the Gyroid cell based TPMS structures.

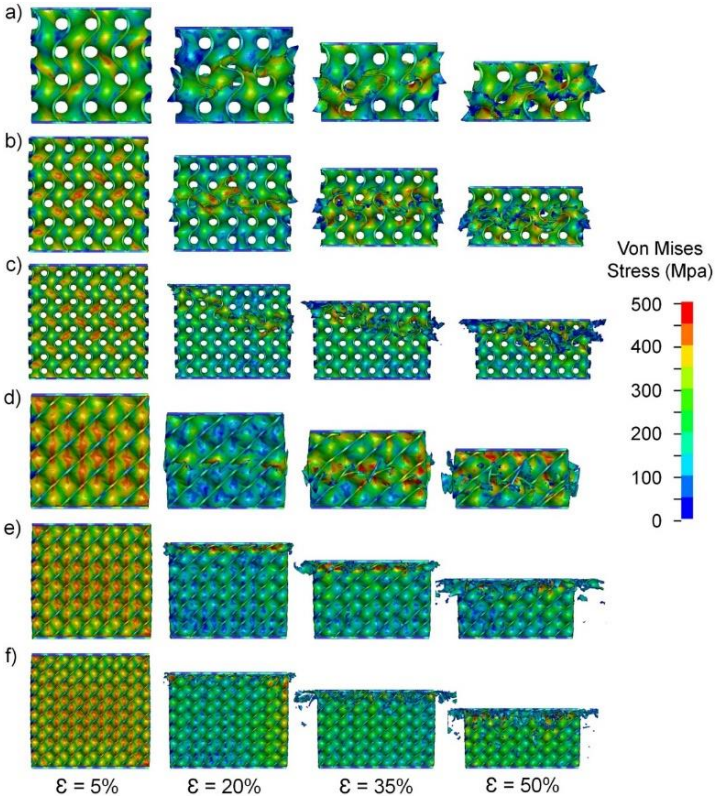

Fig. 10. Comparison of deformation behavior and damage mechanisms at different crushing strains of the TPMS lattice structures at 14.8% and 13.8% relative density: a) G2R3, b) G3R3, c) G4R3, d) D2R2, e) D3R2, and f) D4R2 labeled lattice structures.

It should be noted that the deformation damage mechanisms of the Gyroid and Diamond based TPMS lattice structures are different. The middle cells of the D2R2 labeled TPMS structure are exposed to fracture damage mechanism throughout horizontal cross-section at a crushing strain of 20% (see Figure 10d). This damage mechanism caused a horizontal and progressive collapse starting from the middle cells in the Diamond cell based TPMS structure. However, based on an increment in the cell number, the Diamond cell based TPMS lattice structures exhibited a smooth deformation behavior converting the damage mechanism initiating from the upper cells into progressive damage mechanism in the adjacent cell layers (see Figure 10e, f). Therefore, the stress-strain curves were obtained smoother in the Diamond cell based TPMS lattice structures with higher cell numbers under the same relative density (see Figure 8e, f). On the other hand, the magnitude of the stress fluctuation changed depending on stress softening because of local bending in the Diamond cells. The TPMS lattice structures show bulk material behavior in the densification region. Considering the stress-strain curves of the TPMS lattice structures throughout the crushing process, the plateau region continued until the crushing strain of 70% and then the stress values increased significantly in the densification region.

4. Conclusions

This study aimed to examine the energy absorbing and damage behavior under quasi-static compressive load of Gyroid and Diamond cell based TPMS lattice structures manufactured through powder bed fusion technology using AlSi10Mg alloy material. Energy absorbing characteristics and deformation damage mechanisms of the TPMS lattice structures designed with various relative densities depending on the cell wall thickness and cell number parameters were numerically determined using the commercial Ls-Dyna FE software. The results of the numerical analysis were verified by confronting with the test results of the manufactured samples. Based on the findings obtained from this study, the following conclusions are drawn:

1) Peak stress of the TPMS lattice structures goes up with increasing relative density due to an increment in cell wall thickness.
2) When the cell number is increased under the condition of constant relative density, the peak stress ascends considerably in the Gyroid cell based TPMS lattice structures, whereas it doesn't boost clearly in the Diamond cell based TPMS lattice structures.
3) The specific energy absorption ability of the TPMS lattice structures improves significantly with increasing relative density depending on the cell number and cell wall thickness.
4) The Diamond cell based TPMS lattice structures show 50% more specific energy absorption performance than the Gyroid cell based TPMS lattice structures with close relative densities.
5) The TPMS lattice structures exhibit smoother plateau behavior with lower stress fluctuations depending on increments in the number of cells.
6) The Gyroid cell based TPMS lattice structures show damage mechanism in the form of shear to the right or left, depending on the cell numbers due to the brittle fractured damage behavior after 20% deformation strain.
7) The damage mechanisms of the TPMS lattice structures throughout the crushing process play an important role on revealing the plateau stress and energy-absorbing behavior.
8) The specific energy absorbing ability of the Diamond cell based TPMS lattice structures improves through a progressive damage mechanism that occurs due to an increasing number of cells.
9) The mechanical properties (especially peak stress) of the TPMS lattice structures can be predicted truly by the FE crushing analysis.
10) The highest CFE values for the Diamond and Gyroid cell based lattice structures can be obtained as 54% and 51%, respectively.

This study's findings demonstrate that the Gyroid and Diamond cell-based lattice structures are suitability for energy absorbing applications and will allow the design and fabrication of more efficient lightweight components for aerospace, automotive, and defense industries in the future. The TPMS based structures investigated in this study will also contribute to the development of modern composite structures when used as the core material in sandwich panels. The authors aim to optimize by experimentally and numerically examining the energy absorbing characteristics and damage behavior of these TPMS structures with different cellular geometries under dynamic loading.

Acknowledgment

Karadeniz Technical University supported this study. As researchers, we offer our respects to the Karadeniz Technical University.

Nomenclature

EA	: Energy absorption (J)
SEA	: Specific energy absorption (J/g)
δ	: Crushing displacement (m)
δ_T	: Total crushing displacement (m)
m	: Mass (kg)
F	: Force (N)
CFE	: Crush force efficiency (%)
MCF	: Mean crush force (N)

Conflict of Interest Statement

The authors declare that they have no affiliations with or involvement in any entity or organization with any financial interest (such as educational grants; honoraria; membership, employment, consultancies, stock ownership, or other equity interest; and expert testimony or patent-licensing arrangements participation in speakers' bureaus), or non-financial interest (such as affiliations, personal or professional relationships, knowledge or beliefs) in the subject matter or materials involved in this article.

CRediT Author Statement

İsmail Özen: Conceptualization, Software, Methodology, Investigation, Writing - original draft, Data curation, Validation. **Mustafa Aslan:** Writing - review & editing, Supervision, Writing - original draft, Conceptualization.

References

[1] Ozdemir Z, Hernandez-Nava E, Tyas A, Warren JA, Fay SD, Goodall R, et al. Energy absorption in lattice structures in dynamics: Experiments. Int J Impact Eng 2016;89:49–61.

[2] Yang S, Qi C. Blast-resistant improvement of sandwich armor structure with aluminum foam composite. Adv Mater Sci Eng

[3] Imbalzano G, Tran P, Ngo TD, Lee PVS. Three-dimensional modelling of auxetic sandwich panels for localised impact resistance. J Sandw Struct Mater 2017;19:291–316.

[4] Deshpande VS, Fleck NA. Isotropic constitutive models for metallic foams. J Mech Phys Solids 2000;48:1253–83.

[5] Zhao H, Abdennadher S. On the strength enhancement under impact loading of square tubes made from rate insensitive metals. Int J Solids Struct 2004;41:6677–97.

[6] Chen Z, Xie YM, Wu X, Wang Z, Li Q, Zhou S. On hybrid cellular materials based on triply periodic minimal surfaces with extreme mechanical properties. Mater Des 2019;183.

[7] Maskery I, Aboulkhair NT, Aremu AO, Tuck CJ, Ashcroft IA. Compressive failure modes and energy absorption in additively manufactured double gyroid lattices. Addit Manuf 2017;16:24–9.

[8] Maskery I, Aboulkhair NT, Aremu AO, Tuck CJ, Ashcroft IA, Wildman RD, et al. A mechanical property evaluation of graded density Al-Si10-Mg lattice structures manufactured by selective laser melting. Mater Sci Eng A 2016;670:264–74.

[9] Abueidda DW, Elhebeary M, Shiang CS (Andrew), Pang S, Abu Al-Rub RK, Jasiuk IM. Mechanical properties of 3D printed polymeric Gyroid cellular structures: Experimental and finite element study. Mater Des 2019;165.

[10] Ashby MF. The properties of foams and lattices. Philos Trans R Soc A Math Phys Eng Sci 2006;364:15–30.

[11] Maskery I, Sturm L, Aremu AO, Panesar A, Williams CB, Tuck CJ, et al. Insights into the mechanical properties of several triply periodic minimal surface lattice structures made by polymer additive manufacturing. Polymer (Guildf) 2018;152:62–71.

[12] Lei H, Li C, Meng J, Zhou H, Liu Y, Zhang X, et al. Evaluation of compressive properties of SLM-fabricated multi-layer lattice structures by experimental test and μ-CT-based finite element analysis. Mater Des 2019;169.

[13] Kocabaş GB, Çetin E, Yalçınkaya S, Şahin Y. Experimental Comparison of the Energy Absorption Performance of Traditional Lattice and Novel Lattice Filled Tubes. Int J Automot Sci Technol 2023.

[14] Vrana R, Koutny D, Palousek D. Impact resistance of different types of lattice structures manufactured by SLM. MM Sci J 2016;2016:1579–85. https://doi.org/10.17973/MMSJ.2016_12_2016186.

[15] Niendorf T, Brenne F, Schaper M. Lattice structures manufactured by SLM: On the effect of geometrical dimensions on microstructure evolution during processing. Metall Mater Trans B Process Metall Mater Process Sci 2014;45:1181–5.

[16] Amani Y, Dancette S, Delroisse P, Simar A, Maire E. Compression behavior of lattice structures produced by selective laser melting: X-ray tomography based experimental and finite element approaches. Acta Mater 2018;159:395–407.

[17] Zhang L, Feih S, Daynes S, Chang S, Wang MY, Wei J, et al. Energy absorption characteristics of metallic triply periodic minimal surface sheet structures under compressive loading. Addit Manuf 2018;23:505–15.

[18] Alomar Z, Concli F. A Review of the Selective Laser Melting Lattice Structures and Their Numerical Models. Adv Eng Mater 2020;22.

[19] Yang L, Harrysson O, West H, Cormier D. Mechanical properties of 3D re-entrant honeycomb auxetic structures realized via additive manufacturing. Int J Solids Struct 2015;69–70:475–90.

[20] Maconachie T, Leary M, Lozanovski B, Zhang X, Qian M, Faruque O, et al. SLM lattice structures: Properties, performance, applications and challenges. Mater Des 2019;183.

[21] Sun Q, Sun J, Guo K, Wang L. Compressive mechanical properties and energy absorption characteristics of SLM fabricated Ti6Al4V triply periodic minimal surface cellular structures. Mech Mater 2022;166.

[22] Zhao M, Zhang DZ, Liu F, Li Z, Ma Z, Ren Z. Mechanical and energy absorption characteristics of additively manufactured functionally graded sheet lattice structures with minimal surfaces. Int J Mech Sci 2020;167.

[23] Leary M, Mazur M, Williams H, Yang E, Alghamdi A, Lozanovski B, et al. Inconel 625 lattice structures manufactured by selective laser melting (SLM): Mechanical properties, deformation and failure modes. Mater Des 2018;157:179–99.

[24] Ramos H, Santiago R, Soe S, Theobald P, Alves M. Response of gyroid lattice structures to impact loads. Int J Impact Eng 2022;164.

[25] Al-Ketan O, Rowshan R, Abu Al-Rub RK. Topology-mechanical property relationship of 3D printed strut, skeletal, and sheet based periodic metallic cellular materials. Addit Manuf 2018;19:167–83.

[26] Xu W, Yu A, Lu X, Tamaddon M, Wang M, Zhang J, et al. Design and performance evaluation of additively manufactured composite lattice structures of commercially pure Ti (CP–Ti). Bioact Mater 2021;6:1215–22.

[27] Yan C, Hao L, Hussein A, Raymont D. Evaluations of cellular lattice structures manufactured using selective laser melting. Int J Mach Tools Manuf 2012;62:32–8.

[28] Dokumacı E, Aybarç U, Önel K. Effect of Ultrasonic Treatment Parameters on Microstructural and Mechanical Properties of A356 Aluminum Alloy. Int J Automot Sci Technol 2020;4:234–43.

[29] Aliheidari N, Christ J, Tripuraneni R, Nadimpalli S, Ameli A. Interlayer adhesion and fracture resistance of polymers printed through melt extrusion additive manufacturing process. Mater Des 2018;156:351–61.

[30] Lu C, Zhang Y, Aziz M, Wen P, Zhang C, Shen Q, et al. Mechanical behaviors of multidimensional gradient gyroid

structures under static and dynamic loading: A numerical and experimental study. Addit Manuf 2022;59.
[31] Ha NS, Pham TM, Vo NH, Hao H. Dynamic crushing characteristics of bio-inspired minimal surface primitive structures. Compos Struct 2023;304.
[32] Novak N, Al-Ketan O, Krstulović-Opara L, Rowshan R, Abu Al-Rub RK, Vesenjak M, et al. Quasi-static and dynamic compressive behaviour of sheet TPMS cellular structures. Compos Struct 2021;266.
[33] Committee E. Test methods for tension testing of metallic materials. ASTM Int 2011:1–27.
[34] Li Z hua, Nie Y fei, Liu B, Kuai Z zhou, Zhao M, Liu F. Mechanical properties of AlSi10Mg lattice structures fabricated by selective laser melting. Mater Des 2020;192.
[35] Breitenecker F, Kugi A, Troch I. MATHMOD 2015 - Abstract Volume: Content and Preface, 2018.
[36] Lu C, Zhang C, Wen P, Chen F. Mechanical behavior of Al–Si10–Mg gyroid surface with variable topological parameters fabricated via laser powder bed fusion. J Mater Res Technol 2021;15:5650–61.
[37] Lobdell M, Croop B, Lobo H. Comparison of Crash Models for Ductile Plastics. Mater. Sci., 2015.
[38] Wu Y, Sun L, Yang P, Fang J, Li W. Energy absorption of additively manufactured functionally bi-graded thickness honeycombs subjected to axial loads. Thin-Walled Struct 2021;164.
[39] Zhu H, Wang P, Wei D, Si J, Wu Y. Energy absorption of diamond lattice cylindrical shells under axial compression loading. Thin-Walled Struct 2022;181.
[40] Yin H, Liu Z, Dai J, Wen G, Zhang C. Crushing behavior and optimization of sheet-based 3D periodic cellular structures. Compos Part B Eng 2020;182.
[41] Gümrük R, Mines RAW. Compressive behaviour of stainless steel micro-lattice structures. Int J Mech Sci 2013;68:125–39.
[42] Liu J, Song Y, Chen C, Wang X, Li H, Zhou C, et al. Effect of scanning speed on the microstructure and mechanical behavior of 316L stainless steel fabricated by selective laser melting. Mater Des 2020;186.
[43] Bahrami Babamiri B, Askari H, Hazeli K. Deformation mechanisms and post-yielding behavior of additively manufactured lattice structures. Mater Des 2020.
[44] Smith M, Guan Z, Cantwell WJ. Finite element modelling of the compressive response of lattice structures manufactured using the selective laser melting technique. Int J Mech Sci 2013;67:28–41.